On Effect of Information Loss on Fuser Quality and Utility

Qiang Liu and Nageswara S. V. Rao
Computational Sciences and Engineering Division
Oak Ridge National Laboratory
Oak Ridge, TN 37831
Email: {liuq1,raons}@ornl.gov

***Abstract*—We abstract the accuracy performance of any fuser into a fusion quality measure that is within the range $[0, 1]$ and monotonically decreases with increasing errors. Although there are many possible ways to map the actual error to this quality measure, we adopt a mapping function consisting of both concave and convex regions and its parameters can be tuned based on system design requirements. The effect of communication loss over the links from the sensors, where estimates are generated, to the fuser is then considered, and based on the variations of the quality measure with loss, we define the overall fuser utility that characterizes the resilience of a fuser with increasingly adverse communication constraints. Tracking examples are shown to demonstrate the comparative quality and utility performances of several closed-form fusers.**

I. Introduction

We consider a network of sensors with sensing and communication capabilities, which collect information on targets and generate their state estimates, such as position and velocity. The sensors send these state estimates to a remote fusion center periodically, which then combines them to generate global state estimates for the targets of interest. In reality, due to the often adverse communication conditions over the network, for example, the long distances in long-haul networks, the low propagation speed in underwater acoustic networks, or the blockage and fading effects in airborne networks, etc., the messages from the sensors may suffer from random delays and losses, which could negatively impact the accuracy of the fused result. Although information fusion is a viable means to improve the overall target tracking performance, with increasing loss, the total amount of sensor data arriving at the fusion center in a timely manner is increasingly reduced, which would lead to degraded fusion performance.

There have been existing efforts in the literature to address the information loss in tracking and state estimation. In [3] and [11], performances under generic estimation and fusion settings using Kalman filters under variable packet loss rates have been studied. Various approaches have been proposed in our earlier works, notably information-based selective fusion [9], retransmission [10], staggered scheduling [8], and learning-based fusion [6], to counteract the effect of lost or incomplete sensor data. A number of error metrics can describe the accuracy performance, such as the trace of the error covariance matrix, the determinant of the error covariance matrix, or the root-mean-square error (RMSE) of the position component estimate, among others. In this work, instead of evaluating fuser performance using these metrics, we propose an abstraction of the tracking error performance using a fusion quality measure $Q_F \in [0, 1]$ that is a monotonically decreasing function in any of the above tracking error metrics.

A number of high-level quality-measure abstractions can be pursued in information fusion [2], although we focus on a unifying approach that maps well-known tracking accuracy metrics onto the same scale for easy and fair evaluations of the accuracy performance among possibly diverse system configurations. We show that the mapping rule from the actual tracking error $\mathcal{E}$ to its associated measure $Q_F(\mathcal{E})$ should be designed to satisfy the system requirements and also considerations such as the penalties for increasing errors in different operating regions. In particular, we favor a mapping function that consists of both concave and convex regions so that the effect of the most "critical" part in the overall fusion performance corresponds to the steepest descent in Q_F. In addition, we show that the overall convex function $\mathcal{E}(p)$ with respect to the loss rate p results in expanded concave regions in the constructed quality-loss map, and a more resilient fuser has a comparatively wider concave region. Finally, we use a single utility metric U_F to capture the overall tracking performance with increasing loss and compare among different fusers.

The rest of the paper is organized as follows. In Section II, we describe in detail the formulation of the problem and investigate the chosen function that maps the actual error to the quality measure. In Section III, we carry out monotonicity and concavity analysis of the derived quality-loss map, and define the overall utility measure based on the map. After briefly reviewing a few closed form fusers, we show in Section IV the tracking error, quality measure, and utility measure performances with these fusers using two tracking examples. The paper concludes in Section V.

II. Mapping of Error Metrics to Quality Measures

Let $\mathcal{E}$ represent the actual tracking error metric, for example, the root-mean-square error (RMSE) of the fused position estimate, and $Q_F(\mathcal{E})$ be the *mapping function* that maps $\mathcal{E}$ to the quality measure $Q_F \in [0, 1]$. In this section, we describe how to select an appropriate mapping function based on the system requirement on overall tracking accuracy and also design considerations such as the penalty for increasing

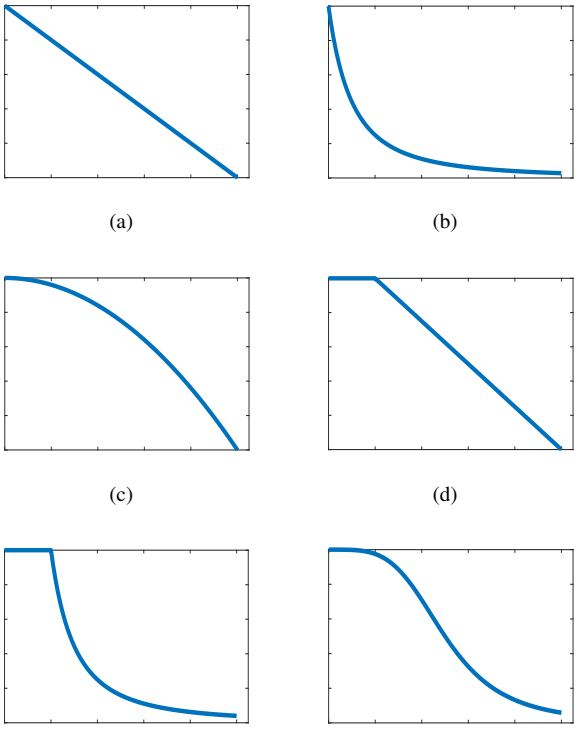

Fig. 1. Candidate mapping functions: (a) linear + zero; (b) convex; (c) concave + zero; (d) one + linear + zero; (e) one + convex; (f) concave + convex

errors. In particular, we investigate monotonicity and concavity conditions of the chosen mapping function and selection of appropriate parameters.

A. Selection of Mapping Function

Fig. 1 shows a list of candidate mapping functions $Q_F(\mathcal{E})$ where the horizontal axes represent the error metric $\mathcal{E}$ and the vertical axes represent the quality measure Q_F. All the candidate functions satisfy the following conditions: (i) $Q_F(0) = 1$; (ii) $Q_f(\infty) = 0$; and (iii) $Q_F(\mathcal{E})$ is a non-increasing function in $\mathcal{E}$. The linear function in Fig. 1a and the concave function in Fig. 1c both lead to zero quality measure at finite $\mathcal{E}$ values; on the other hand, the convex mapping in Fig. 1b penalizes small $\mathcal{E}$ values since it features the most significant reduction in the quality measure in that region. Figs. 1d and 1e show modified linear and convex mapping functions respectively in which the first portion, corresponding to the smallest errors, stays at 1; nevertheless, they still do not eliminate the above issues entirely besides introducing a "kink" in the function where it is non-differentiable. Finally, Fig. 1f shows a mapping function that features a concave region followed by a convex region and overall has the best characteristics: (i) smooth everywhere; (ii) monotonically decreasing; and (iii) the reduction in Q_F is most prominent in the "middle" portion corresponding to the most precipitous drop, while the quality drops very slowly in regions with extremely small or extremely large errors.

To select a curve that has the shape of an inverted S-shape like that shown in Fig. 1f, the most obvious choices

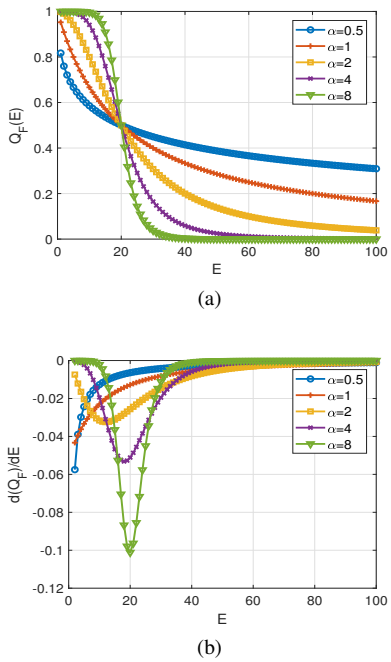

Fig. 2. Plots of (a) Q_F and (b) $\frac{dQ_F}{d\mathcal{E}}$ with $\beta = 1$ and variable α choices

are modified sigmoid or logistic functions that can indeed approximate our desired mapping functions. However, those functions are defined over $(-\infty, \infty)$, and we instead consider using a different function that is defined on $[0, \infty)$:

$$Q_F(\mathcal{E}) = \left(1 + \left(\frac{\mathcal{E}}{\mathcal{E}_r}\right)^{\alpha}\right)^{-\beta}, \tag{1}$$

where $0 < \mathcal{E}_r < \infty$ is a reference error point and both $\alpha > 0$ and $\beta > 0$ are parameters to be determined.

B. Characteristics of Our Mapping Function

Regardless of α and β choices in Eq. (1), one can easily see that (i) $Q_F(0) = 1$; (ii) $Q_F(\infty) = 0$; and (iii) $Q_F(\mathcal{E}_r) = 2^{-\beta}$. To visualize the behavior of the mapping function, we first plot $Q_F(\mathcal{E})$ with a number of α choices while $\beta = 1$ and the reference error point is set to be $\mathcal{E}_r = 20$. As shown in Fig. 2a, smaller α values (e.g., 0.5 and 1) lead to entirely convex profiles whereas increasing α can result in a more noticeable concave to convex transition and a sharper transition in quality from one to zero. These can be confirmed by their respective derivative curves plotted in Fig. 2b, in which the minimum (between monotonically decreasing and increasing portions of a curve) indicates the transition from concave to convex regions. It can be seen that, with increasing α, the transition point moves closer to the reference error $\mathcal{E}_r$. On the other hand, if we set $\alpha = 4$ and vary β values, the plots in Fig. 3 show that with increasing β, the concave to convex transition point also shifts left, toward smaller $\mathcal{E}$ values, and overall the transition features a sharper drop in Q_F.

We state the above observations formally in the proposition below.

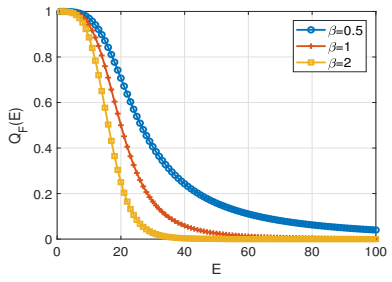

(a)

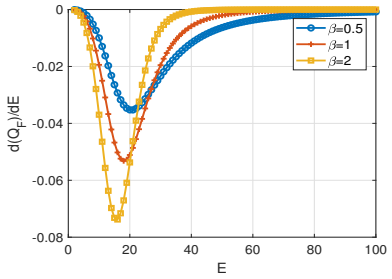

(b)

Fig. 3. Plots of (a) Q_F and (b) $\frac{dQ_F}{d\mathcal{E}}$ with $\alpha = 4$ and variable β choices

Proposition 1. *The mapping function in Eq.* (1) *is a monotonically decreasing function over* $[0, \infty)$*; when* $\alpha > 1$ *and* $\beta \geq 1$*, it has a single inflection point at* $\mathcal{E} = \left(\frac{\alpha-1}{\alpha\beta+1}\right)^{\frac{1}{\alpha}}\mathcal{E}_r$ *where the function switches from being concave to convex, and this point monotonically increases with* α *and decreases with* β*.*

Proof. From Eq. (1), we take the derivative of the mapping function and have

$$Q'_F(\mathcal{E}) = \frac{d}{d\mathcal{E}}Q_F(\mathcal{E}) = \frac{-\alpha\beta}{\mathcal{E}_r}\left(1+\left(\frac{\mathcal{E}}{\mathcal{E}_r}\right)^{\alpha}\right)^{-\beta-1}\left(\frac{\mathcal{E}}{\mathcal{E}_r}\right)^{\alpha-1}. \tag{2}$$

It is apparent that $Q'_F(0) = 0$ and $Q'_F(\mathcal{E}_r) = \frac{-\alpha\beta}{\mathcal{E}_r} \times 2^{-\beta-1}$. Let

$$g(\mathcal{E}) = \left(\frac{\mathcal{E}}{\mathcal{E}_r}\right)^{\alpha-1},$$

and

$$h(\mathcal{E}) = \left(1+\left(\frac{\mathcal{E}}{\mathcal{E}_r}\right)^{\alpha}\right)^{\beta+1}.$$

Apparently

$$Q'_F(\mathcal{E}) = \frac{-\alpha\beta}{\mathcal{E}_r}\frac{g(\mathcal{E})}{h(\mathcal{E})}.$$

Now, since $\lim_{\mathcal{E}\to\infty} g(\mathcal{E}) = \infty$ and $\lim_{\mathcal{E}\to\infty} h(\mathcal{E}) = \infty$, using L'Hospital's Rule, we have

$$\begin{aligned}
\lim_{\mathcal{E}\to\infty}\frac{g(\mathcal{E})}{h(\mathcal{E})} &= \lim_{\mathcal{E}\to\infty}\frac{g'(\mathcal{E})}{h'(\mathcal{E})} \\
&= \lim_{\mathcal{E}\to\infty}\frac{\frac{1}{\mathcal{E}_r}(\alpha-1)\left(\frac{\mathcal{E}}{\mathcal{E}_r}\right)^{\alpha-2}}{\frac{1}{\mathcal{E}_r}\alpha(\beta+1)\left(\frac{\mathcal{E}}{\mathcal{E}_r}\right)^{\alpha-1}\left(1+\left(\frac{\mathcal{E}}{\mathcal{E}_r}\right)^{\alpha}\right)^{\beta}} \\
&= \frac{\alpha-1}{\alpha(\beta+1)}\lim_{\mathcal{E}\to\infty}\frac{1}{\left(\frac{\mathcal{E}}{\mathcal{E}_r}\right)\left(1+\left(\frac{\mathcal{E}}{\mathcal{E}_r}\right)^{\alpha}\right)^{\beta}} \\
&= 0,
\end{aligned}$$

and then $Q'_F(\infty) = 0$. From Eq. (2), for all $\mathcal{E} \in (0, \infty)$, $Q'_F(\mathcal{E}) < 0$, and hence $Q_F(\mathcal{E})$ is a monotonically decreasing function.

To show the concavity/convexity of Q_F, we consider its second derivative, which can be calculated as

$$\begin{aligned}
Q''_F(\mathcal{E}) &= \frac{d}{d\mathcal{E}}Q'_F(\mathcal{E}) \\
&= \frac{\alpha\beta}{\mathcal{E}_r^2}\left(1+\left(\frac{\mathcal{E}}{\mathcal{E}_r}\right)^{\alpha}\right)^{-\beta-2}\left(\frac{\mathcal{E}}{\mathcal{E}_r}\right)^{\alpha-2} \times \\
&\qquad \left[(\alpha\beta+1)\left(\frac{\mathcal{E}}{\mathcal{E}_r}\right)^{\alpha} - (\alpha-1)\right].
\end{aligned} \tag{3}$$

From Eq. (3), we can easily obtain $Q''_F(0) = 0$ and $Q''_F(\mathcal{E}_r) = \frac{\alpha\beta}{\mathcal{E}_r^2}[\alpha(\beta-1)+2]\cdot 2^{-\beta-2}$. The derivation of $Q''_F(\infty)$ is somewhat more involved, although we can still apply L'Hospital's Rule as before on both of the expanded terms in Eq. (3), and obtain $Q''_F(\infty) = 0$.

Now, if we let $Q''_F(\mathcal{E}) = 0$ and solve for $\mathcal{E}$, besides $\mathcal{E} = 0, \infty$, another point $\mathcal{E}_T = \left(\frac{\alpha-1}{\alpha\beta+1}\right)^{\frac{1}{\alpha}}$ also satisfies the condition. Moreover, for all $\mathcal{E} \in (0, \mathcal{E}_T)$, $Q''_F(\mathcal{E}) < 0$ whereas $Q''_F(\mathcal{E}) > 0$ for all $\mathcal{E} \in (\mathcal{E}_T, \infty)$. Therefore, $\mathcal{E}_T$ is an inflection point of Q_F at which the function changes from being concave to convex. Finally, suppose

$$f(\alpha, \beta) = \left(\frac{\alpha-1}{\alpha\beta+1}\right)^{\frac{1}{\alpha}}.$$

It is easy to show that

$$\frac{\partial f}{\partial \beta} = -\frac{1}{\alpha\beta+1}\left(\frac{\alpha-1}{\alpha\beta+1}\right)^{\frac{1}{\alpha}} < 0;$$

that is, the inflection point $\mathcal{E}_T = \mathcal{E}_r f(\alpha, \beta)$ monotonically decreases with β. To calculate the partial derivative of f with respect to α, we first need to take the logarithms on both sides. After some algebraic manipulation, we obtain

$$\frac{\partial f}{\partial \alpha} = \left(\frac{\alpha-1}{\alpha\beta+1}\right)^{\frac{1}{\alpha}}\left[\frac{1+\beta}{\alpha(\alpha-1)(\alpha\beta+1)} - \frac{1}{\alpha^2}\ln\left(\frac{\alpha-1}{\alpha\beta+1}\right)\right].$$

Now, since $\alpha > 1$ and $\beta \geq 1$, we have $0 < \alpha - 1 < \alpha\beta + 1$ so that $\ln\left(\frac{\alpha-1}{\alpha\beta+1}\right) < 0$ and in turn $\frac{\partial f}{\partial \alpha} > 0$. In other words, the inflection point $\mathcal{E}_T$ monotonically increases with α and in the extreme cases,

$$\mathcal{E}_T(\alpha, \beta)\Big|_{\alpha\to 1} = 0 \text{ and } \mathcal{E}_T(\alpha, \beta)\Big|_{\alpha\to\infty} = \mathcal{E}_r.$$

□

C. Selection of Appropriate α and β Values

So far we have not considered the detailed setup of α and β parameters in the mapping function. Recall from the plots in Figs. 2 and 3 and also the discussions in the previous subsection, for the same reference error $\mathcal{E}_r$, increasing α and/or decreasing β would lead to sharper transitions from concave to convex mappings. Now, suppose the reference error overlaps the *highest* tracking error that the system tolerates; i.e., $\mathcal{E}_r = \mathcal{E}_H$. If we let Q_L denote the *lowest* quality measure corresponding to this error, i.e., $Q_L = Q_F(\mathcal{E}_H)$, then from Eq. (1), we have $Q_L = 2^{-\beta}$, or equivalently

$$\beta = \frac{\ln\left(\frac{1}{Q_L}\right)}{\ln 2}. \tag{4}$$

Typically, we have $Q_L \leq 0.5$ such that $\beta \geq 1$. By setting the inflection point $\mathcal{E}_T$ in such a way, we penalize the error increases leading up to $\mathcal{E}_H$ by rapidly decreasing Q_F values.

On the other hand, to determine the value of α, the system can also specify another pair of parameters as a reference point: $\mathcal{E}_L$, the *lowest* achievable error, and Q_H, the *highest* achievable quality corresponding to this error. Note that due to system uncertainty, even the best fuser cannot achieve zero estimation error, or equivalently, a quality measure that equals one. A statement like "The quality of a $1\,\mathrm{m}$ estimation error is 99 out of 100" is equivalent to $\mathcal{E}_L = 1\,\mathrm{m}$ and $Q_H = 0.99$. Plugging $(\mathcal{E}_L, Q_H)$ into Eq. (1), we have $Q_H = (1 + (\mathcal{E}_L/\mathcal{E}_H)^{\alpha})^{-\beta}$; then α can be solved for as

$$\alpha = \frac{\ln\left[\left(\frac{1}{Q_H}\right)^{\frac{1}{\beta}} - 1\right]}{\ln\left(\frac{\mathcal{E}_L}{\mathcal{E}_H}\right)} = \frac{\ln\left[\left(\frac{1}{Q_H}\right)^{\frac{\ln 2}{\ln\left(\frac{1}{Q_L}\right)}} - 1\right]}{\ln\left(\frac{\mathcal{E}_L}{\mathcal{E}_H}\right)}. \tag{5}$$

Now, since we need $\alpha > 1$ for initial concave mapping, from Eq. (5), we have $\left(\frac{1}{Q_H}\right)^{\frac{\ln 2}{\ln\left(\frac{1}{Q_L}\right)}} - 1 < \frac{\mathcal{E}_L}{\mathcal{E}_H}$ (since both are within $(0,1)$ and therefore their logarithms are negative). Reorganizing this inequality, we have

$$\mathcal{E}_L > \mathcal{E}_H\Big[\Big(\frac{1}{Q_H}\Big)^{\frac{\ln 2}{\ln\left(\frac{1}{Q_L}\right)}} - 1\Big]; \tag{6}$$

or, equivalently,

$$Q_H > \Big(1 + \frac{\mathcal{E}_L}{\mathcal{E}_H}\Big)^{-\frac{\ln\left(\frac{1}{Q_L}\right)}{\ln 2}}. \tag{7}$$

III. Fuser Quality-Loss Map and Utility

In this section, we consider the effect of communication loss on the fusion quality measure by constructing the quality-loss, or Q-p map, where p denotes the loss rate. We also propose the utility measure U_F to quantitatively describe the overall resilience of a fuser against increasing errors.

A. Q-p Map

Let the error performance metric $\mathcal{E}$ be a function of the loss rate $p \in [0,1]$, i.e., $\mathcal{E}(p)$. The increase in p corresponds to increasingly unavailable sensor estimates, upon which a fuser may exclude the sensor(s) with missing estimates at time of fusion, or use its own predicted estimates to substitute the missing ones. Obviously, $\mathcal{E}(p)$ is a monotonically increasing function in p and $\mathcal{E}(1) = \infty$ corresponds to the extreme case where no sensor data are present; in other words, the derivative of $\mathcal{E}$ with respect to p satisfies $\mathcal{E}'(p) = \frac{d\mathcal{E}}{dp} > 0$ for $p \in (0,1)$. Furthermore, by intuition, the rate of increase in $\mathcal{E}(p)$ should increase with p as well, i.e., $\mathcal{E}''(p) = \frac{d^2\mathcal{E}}{dp^2} > 0$ for $p \in (0,1)$ to reflect the increasingly adverse effect of missing estimates on tracking accuracy, as has been evidenced in our earlier studies and also works such as [3].

In the following discussions, without further specification, we use the notation "Q" and "Q_F" interchangeably to refer to the quality measure we defined in the previous section. We now consider the composite function $Q(\mathcal{E}(p)) : [0,1] \mapsto [0,1]$ that maps $\mathcal{E}(p)$ onto the quality measure. We refer to the plot of Q_F versus p as the Q-p map, and in the rest of this section, we qualitatively analyze the behavior of the Q-p map.

First, using the chain rule, we have

$$\frac{dQ}{dp} = \frac{dQ}{d\mathcal{E}}\frac{d\mathcal{E}}{dp} < 0, \tag{8}$$

for all $p \in (0,1)$; in other words, the fusion quality measure Q_F is a monotonically decreasing function with the loss rate p. Taking the derivatives again on both sides of Eq. (8), using the chain rule, we have

$$\frac{d^2Q}{dp^2} = \frac{d^2Q}{d\mathcal{E}^2}\Big(\frac{d\mathcal{E}}{dp}\Big)^2 + \frac{dQ}{d\mathcal{E}}\frac{d^2\mathcal{E}}{dp^2}. \tag{9}$$

We consider the following cases:

- When $\mathcal{E}(p) < \mathcal{E}_T$, from the previous section, we have $\frac{d^2Q}{d\mathcal{E}^2} < 0$. In addition, in Eq. (9), $\left(\frac{d\mathcal{E}}{dp}\right)^2 > 0$, $\frac{dQ}{d\mathcal{E}} < 0$, and due to the convexity of $\mathcal{E}(p)$, $\frac{d^2\mathcal{E}}{dp^2} > 0$. As a result, we have $\frac{d^2Q}{dp^2} < 0$; i.e., for $p \in (0, p_{\mathcal{E}_T})$ where $\mathcal{E}(p_{\mathcal{E}_T}) = \mathcal{E}_T$, the Q-p map is concave.
- When $p = p_{\mathcal{E}_T}$, $\mathcal{E}(p) = \mathcal{E}_T$, and we have $\frac{d^2Q}{d\mathcal{E}^2} = 0$; then from Eq. (9), $\frac{d^2Q}{dp^2} = \frac{dQ}{d\mathcal{E}}\frac{d^2\mathcal{E}}{dp^2} < 0$. In other words, at $p = p_{\mathcal{E}_T}$, the Q-p map is still concave.
- For $p \in (p_{\mathcal{E}_T}, 1)$, the associated errors are in the convex zone when mapped to Q_F; i.e., $\frac{d^2Q}{d\mathcal{E}^2} > 0$. And Eq. (9), now the sum of positive and negative terms, does not lead directly to a definite sign of $\frac{d^2Q}{dp^2}$. Due to the continuity of the individual derivatives in Eq. (9), however, $\frac{d^2Q}{dp^2}$ must be initially negative; in addition, from Eq. (8), in order for Q_F to continue decreasing monotonically, it must switch to convex at a certain point so that Q_F will remain strictly positive for all $p < 1$. Therefore, the concave to convex transition point of the Q-p map p_T must occur here and we have $p_T > p_{\mathcal{E}_T}$ and $\mathcal{E}(p_T) > \mathcal{E}_T$.

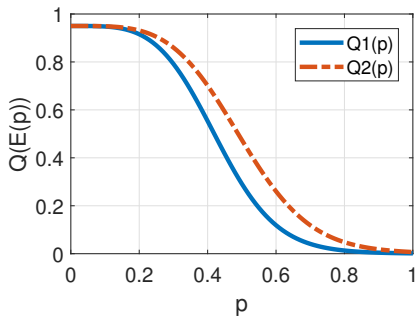

Fig. 4. Two Q-p map profiles with different utilities

B. Fuser Utility

The discussions above have assumed the fact that a fuser is good enough to yield a quality measure Q_F at zero loss, namely, well within the concave region of the mapping function; for example, $Q(\mathcal{E}(0))$ should be reasonably close to Q_H in Eq. (7). In addition, we showed that the Q-p map has an extended concave region in terms of the tracking error at the transition point.

We now consider the two Q-p map profiles shown in Fig. 4. Both start with identical lossless quality measures at $Q_F = 0.95$. Compared to the curve labeled as Q_1, the Q_2-p map exhibits an expanded concave region, where the transition occurs around $p_T = 0.5$ as opposed to that around 0.4 for the Q_1-p map. The profile of the Q_2-p map is more desirable since the quality measure Q_F sustains longer with increasing loss due to its expanded concave region. We account for the overall profile of the Q-p maps by defining its fuser utility measure U_F as

$$U_F = \int_{p=0}^{1} Q(p)dp, \tag{10}$$

which is simply $\bar{Q}$, the mean of Q_F, or the area under the curve in the Q-p map. This utility measure enables us to quantitatively compare the performance of two fusers in terms of their resilience against increasing loss; with comparable lossless error performances, a more resilient fuser typically exhibits a longer concave region, thereby leading to a higher U_F value.

IV. Fuser Quality and Utility Performance

In this section, we investigate the Q_F and U_F performances of three closed-form fusers in two target tracking scenarios: (i) a simple target whose motion is approximately along a straight line; and (ii) a motion-constrained maneuvering target that moves along an elliptical track. In particular, we compare the accuracy performances among the three fusers in either case and use the utility measure U_F to demonstrate their respective resilience against increasing link-level loss.

A. Fusers

Without loss of generality, we focus on two-sensor fusion scenarios in the rest of the paper, although the results can be readily extended to cases involving more sensors.

1) Average Fuser: The simplest average fuser (AF) calculates the arithmetic mean of the sensor estimates as the fuser output:

$$\mathbf{P}_k^G = \frac{1}{2}(\mathbf{P}_k^1 + \mathbf{P}_k^2), \tag{11}$$

$$\hat{\mathbf{x}}_k^G = \frac{1}{2}(\hat{\mathbf{x}}_k^1 + \hat{\mathbf{x}}_k^2), \tag{12}$$

in which the superscript "G" denotes the global estimate at the fusion center.

2) Simple Track-to-Track Fuser: The simple track-to-track fuser (T2TF) is a convex combination of the sensor estimates as follows [1]:

$$(\mathbf{P}_k^G)^{-1} = (\mathbf{P}_k^1)^{-1} + (\mathbf{P}_k^2)^{-1}, \tag{13}$$

$$\hat{\mathbf{x}}_k^G = \mathbf{P}_k^G \left((\mathbf{P}_k^1)^{-1}\hat{\mathbf{x}}_k^1 + (\mathbf{P}_k^2)^{-1}\hat{\mathbf{x}}_k^2\right). \tag{14}$$

It is well known that the common process noise results in correlation in the error cross-covariance across sensor estimates. However, it is generally difficult to derive the exact cross-covariances over time; as a result, one may assume that the cross-covariance is negligible in order to apply this simplified fuser, even though the result will be suboptimal.

3) Fast Covariance Intersection Fuser: Another fusion method without knowledge of the cross-covariance information is the covariance intersection (CI) algorithm. The intuition behind this approach comes from a geometric interpretation of the problem. If one were to plot the covariance ellipses for $\mathbf{P}_F$ (defined as the locus of points $\{\mathbf{y} : \mathbf{y}^T\mathbf{P}_F^{-1}\mathbf{y} = c\}$ where c is some constant), the ellipses of $\mathbf{P}_F$ are found to always contain the intersection of the ellipses for $\mathbf{P}_1$ and $\mathbf{P}_2$ for all possible choices of $\mathbf{P}_{12}$ [5]. The method is characterized by the weighted convex combination of sensor covariances:

$$(\mathbf{P}_k^G)^{-1} = \omega_1(\mathbf{P}_k^1)^{-1} + \omega_2(\mathbf{P}_k^2)^{-1}, \tag{15}$$

$$\hat{\mathbf{x}}_k^G = \mathbf{P}_k^G \left(\omega_1(\mathbf{P}_k^1)^{-1}\hat{\mathbf{x}}_k^1 + \omega_2(\mathbf{P}_k^2)^{-1}\hat{\mathbf{x}}_k^2\right), \tag{16}$$

where $\omega_1, \omega_2 > 0$ ($\omega_1 + \omega_2 = 1$) are weights to be determined (e.g., by minimizing the determinant of $\mathbf{P}_k^G$). A fast CI algorithm is proposed in [12] where the weights are found based on an information-theoretic criterion so that ω_1 and ω_2 can be solved for analytically as follows:

$$\omega_1 = \frac{D(p_1, p_2)}{D(p_1, p_2) + D(p_2, p_1)}, \tag{17}$$

where $D(p_A, p_B)$ is the Kullback-Leibler (KL) divergence from $p_A(\cdot)$ to $p_B(\cdot)$, and

$$\omega_2 = 1 - \omega_1. \tag{18}$$

When the underlying estimates are Gaussian, the KL divergence at time k can be computed as

$$D_k(p_i, p_j) = \frac{1}{2}\left[\ln\frac{|\mathbf{P}_k^j|}{|\mathbf{P}_k^i|} + \mathbf{d}_{k,i\to j}^T(\mathbf{P}_k^j)^{-1}\mathbf{d}_{k,i\to j} + Tr(\mathbf{P}_k^i(\mathbf{P}_k^j)^{-1}) - n\right], \tag{19}$$

where $\mathbf{d}_{k,i\to j} = \hat{\mathbf{x}}_k^i - \hat{\mathbf{x}}_k^j$, n is the dimensionality of the state, and $|\cdot|$ denotes the determinant.

B. Tracking Scenario #1: Straight-Line Target

In the first example, we show tracking error performance of a 2D target whose trajectory is approximately a straight line.

1) Discretized Continuous White-Noise Acceleration (CWNA) Model: The discretized CWNA model is a simple, commonly used model in which an object moving in a generic coordinate system $\xi - \eta$ is assumed to be traveling at a nearly constant speed. The discrete-time state equation is given by $\mathbf{x}_{k+1} = \mathbf{F}\mathbf{x}_k + \mathbf{w}_k$, where (dropping the time index k), $\mathbf{x} = [\xi \quad \dot{\xi} \quad \eta \quad \dot{\eta}]^T$ is a vector (with "T" denoting the transpose) consisting of the position and velocity components in both coordinates. The transition matrix $\mathbf{F}$ is given by

$$\mathbf{F} = \begin{bmatrix} \begin{bmatrix} 1 & T \\ 0 & 1 \end{bmatrix} & \mathbf{0}_{2\times 2} \\ \mathbf{0}_{2\times 2} & \begin{bmatrix} 1 & T \\ 0 & 1 \end{bmatrix} \end{bmatrix}, \tag{20}$$

where T is the sample period. The covariance of the discrete-time process noise $\mathbf{w}_k$ is

$$\mathbf{Q} = \begin{bmatrix} \tilde{q}_\xi \begin{bmatrix} T^3/3 & T^2/2 \\ T^2/2 & T \end{bmatrix} & \mathbf{0}_{2\times 2} \\ \mathbf{0}_{2\times 2} & \tilde{q}_\eta \begin{bmatrix} T^3/3 & T^2/2 \\ T^2/2 & T \end{bmatrix} \end{bmatrix}. \tag{21}$$

where $\tilde{q}_\xi$ and $\tilde{q}_\eta$ are respectively the power spectral densities (PSDs) of the underlying continuous-time white stochastic process along either coordinate.

2) Generating Target States and Sensor Estimates: The state space is initialized as

$$[\xi_0 \quad \dot{\xi}_0 \quad \eta_0 \quad \dot{\eta}_0]^T \sim \mathcal{N}([260 \quad 60 \quad 260 \quad 60]^T, \mathrm{diag}\{625, 100, 625, 100\})$$
$$\mathbf{x}_0 = [\xi_0 \quad \dot{\xi}_0 \quad \eta_0 \quad \dot{\eta}_0]^T$$

and the process noise PSDs $\tilde{q}_\eta$ and $\tilde{q}_\eta$ is set to be $0.02\,\mathrm{m}^2/\mathrm{s}^3$ with a sampling period of $T = 2\,\mathrm{s}$. Two sensors are used to observe the target motion where the direct position measurements are generated with the standard deviations of the measurement errors being $40\,\mathrm{m}$ and $25\,\mathrm{m}$ respectively. Kalman filters are run recursively to generate the state estimates.

3) Quality and Utility Performance: Table I lists the position estimate root-mean-square errors (RMSEs) of both sensors and various fusers, where for the latter the communication links between the sensors and the fusion center have been assumed to be lossless. Note the track-to-track fuser (T2TF) outperforms the covariance-intersection (CI) fuser, which in turn slightly outperforms the average fuser (AF). On the other hand, Fig. 5 plots their errors with increasing link loss rates, where one can easily observe the overall convexity of the error curves. Once the loss rate exceeds a certain level, the effect of error divergence (e.g., due to prediction) will become more prominent. To map these errors to an appropriate quality measure Q_F, in Table II, we list two options, both with $\mathcal{E}_H$, the highest tolerable error, set to be $20\,\mathrm{m}$. The Q_L values for this reference error are set to be 0.5 and 0.3 respectively for the two cases, reflecting the more stringent requirement of the latter. Meanwhile, from the table, another reference point, namely, the $(\mathcal{E}_L, Q_H)$ pair, is set to be $(5, 0.98)$ and $(3, 0.99)$ respectively. From these system parameters, we can calculate the α and β values for the desired mapping functions and can also derive the error corresponding to the inflection point according to Proposition 1, as listed in the table.

TABLE I
POSITION ESTIMATE ROOT-MEAN-SQUARE ERROR (RMSE) PERFORMANCE (IN m)

sensor/fuser	Sensor 1	Sensor 2	AF	T2TF	CI
RMSE	20.9	14.0	13.3	12.3	13.1

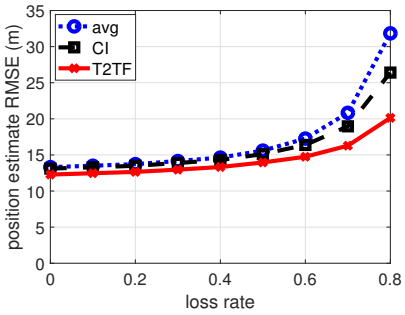

Fig. 5. RMSE performance of fused position estimates with loss rates

TABLE II
SELECTION OF TWO MAPPING FUNCTIONS

case	$(\mathcal{E}_H, Q_L)$	$(\mathcal{E}_L, Q_H)$	β	α	$\mathcal{E}_T$
1	$(20, 0.5)$	$(5, 0.98)$	1	2.142	15.3
2	$(20, 0.3)$	$(3, 0.99)$	1.373	2.714	12.8

Once we have the mapping function, then the Q-p map for that particular function can be drawn. Figs. 6a and 6b show the maps for the above two cases respectively. The overall lower Q_F profiles in the latter demonstrate the more stringent requirement in the system parameters (i.e., higher penalty for the same error). Besides, one can notice the predominantly concave profiles followed by convex profiles when the loss rate becomes high. The transition points p_T from being concave to convex are observed to be around 80% to 90% loss range, whose corresponding errors ($> 20\,\mathrm{m}$) are all well above the $\mathcal{E}_T$ values in Table II, as we have discussed in Section III. Finally, the composite utility U_F bar graph in Fig. 6c shows the overall utility of the fusers as calculated according to Eq. (10). All three fusers, despite performance differences, yield U_F values of over 0.5 in the first case, while those values are all below 0.5 for the second case stemming from the lower Q_L choice for the latter.

C. Tracking Scenario #2: Constrained Maneuvering Target

In this tracking example, we consider a maneuvering target whose motion is constrained by a known ellipse. Due to the nonlinearity of the target trajectory, we adopt the nonlinear coordinated turn (CT) model to describe target state evolution. Extended Kalman filters (EKFs) are run by the sensors to generate state estimates. Moreover, due to the presence of the

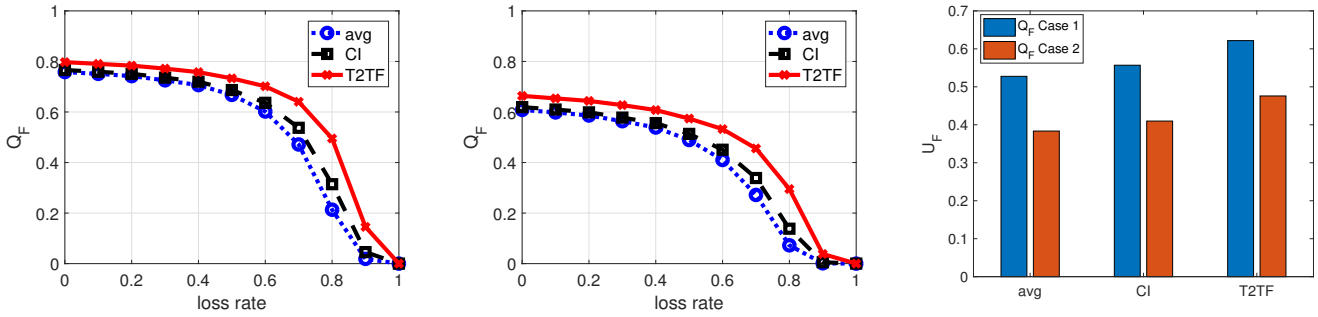

(a) Q-p map: Case 1 (b) Q-p map: Case 2 (c) U_F: Composite

Fig. 6. Performance of fused position estimates with two different mapping functions

constraint, after fusing sensor estimates, the fuser may carry out an additional projection step so that the unconstrained fused estimates can be projected onto the elliptical constraint.

1) Coordinated Turn (CT) Model: A maneuver usually follows a *coordinated turn* (CT) pattern characterized by a near constant turn rate and near constant speeds along both coordinates. If we add the turn rate component Ω to the state vector: $\mathbf{x} = \begin{bmatrix}\xi & \dot{\xi} & \eta & \dot{\eta} & \Omega\end{bmatrix}^T$, the state evolution is described by the following discretized CT model [1]:

$$\begin{aligned}\mathbf{x}_{k+1} &= \mathbf{F}_k\mathbf{x}_k + \mathbf{w}_k \\ &= \begin{bmatrix} 1 & \frac{\sin\Omega_k T}{\Omega_k} & 0 & -\frac{1-\cos\Omega_k T}{\Omega_k} & 0 \\ 0 & \cos\Omega_k T & 0 & -\sin\Omega_k T & 0 \\ 0 & \frac{1-\cos\Omega_k T}{\Omega_k} & 1 & \frac{\sin\Omega_k T}{\Omega_k} & 0 \\ 0 & \sin\Omega_k T & 0 & \cos\Omega_k T & 0 \\ 0 & 0 & 0 & 0 & 1 \end{bmatrix}\mathbf{x}_k + \mathbf{w}_k,\end{aligned} \tag{22}$$

where the covariance matrix of the process noise $\mathbf{w}_k$ is given by

$$\mathbf{Q}_k = \begin{bmatrix} \tilde{q}_\xi \begin{bmatrix} T^3/3 & T^2/2 \\ T^2/2 & T \end{bmatrix} & \mathbf{0}_{2\times 2} & \begin{matrix} 0 \\ 0 \end{matrix} \\ \mathbf{0}_{2\times 2} & \tilde{q}_\eta \begin{bmatrix} T^3/3 & T^2/2 \\ T^2/2 & T \end{bmatrix} & \begin{matrix} 0 \\ 0 \end{matrix} \\ \begin{matrix} 0 & 0 \end{matrix} & \begin{matrix} 0 & 0 \end{matrix} & \tilde{q}_\Omega T \end{bmatrix}, \tag{23}$$

in which $\tilde{q}_\Omega$ is the noise PSD of the turn rate component.

2) Generating Target States and Sensor Estimates: Suppose the target trajectory satisfies the following elliptical constraint:

$$\frac{(\xi_k - \xi_c)^2}{a^2} + \frac{(\eta_k - \eta_c)^2}{b^2} = 1, \tag{24}$$

where (ξ_c, η_c) is the center of the ellipse, a and b are respectively the radii along the ξ and η axes, and for simplicity, the major and minor axes of the ellipsis are aligned with the ξ and η axes. Taking the derivative of the position constraint, we have the constraint on the velocity as

$$\frac{\xi_k - \xi_c}{a^2}\dot{\xi}_k + \frac{\eta_k - \eta_c}{b^2}\dot{\eta}_k = 0. \tag{25}$$

We can generate target states that satisfy the above constraints in two steps: (1) generate states constrained by the unit circle $\xi^2 + \eta^2 = 1$; (2) transform these states to their elliptical constrained counterparts by means of translation and non-uniform scaling. In particular, for the first step, a method is proposed in [4] that utilizes the traveled distance along the circular track and its change rate to generate constrained position and velocity components. More detailed discussions can be found in [7].

The center of the elliptical track is set at $(\xi_c, \eta_c) = (2000, 1000)\,\mathrm{m}$ with radii along the axes $a = 1500\,\mathrm{m}$ and $b = 800\,\mathrm{m}$. The initial state of the target is generated around $\mathbf{x}_0 = (\xi_c + a, \eta_c, 0, v_0, v_0/a)$ where $v_0 = 25\,\mathrm{m/s}$; that is, the initial position is centered around $(\xi_c + a, \eta_c)$ and the mean magnitude of the initial velocity is v_0. To account for the system nonlinearity, both sensors are initialized with sufficiently large error covariances and run EKF on top of the CT model with appropriately tuned parameters, i.e., the process noise PSDs $\tilde{q}_\xi$, $\tilde{q}_\eta$, and $\tilde{q}_\Omega$ that reflect the level of process noise in the target state generation. For direct position measurements, in contrast to the previous linear tracking case, measurement mean standard deviations along both axes are set to be $20\,\mathrm{m}$ and $15\,\mathrm{m}$ respectively for the two sensors.

3) Generating Projected Fused Estimate: After the sensors send their state estimates to the fusion center, the fuser first combines them to generate a fused unconstrained estimate; then, this unconstrained estimate can be projected onto the known constraint by certain distance-based criteria. For example, in [7], we proposed finding the point on the ellipse that is closest to the unconstrained estimate by solving a quartic equation, where the real solution with the smallest absolute value corresponds to the minimum-distance point on the ellipse. Such constrained fused estimates have been shown to outperform their unconstrained counterparts in terms of overall tracking accuracy.

4) Quality and Utility Performance: Similar to the linear tracking case, we first investigate the error performance in Fig. 7a, in which both unconstrained and constrained (shown as "-proj" cases in the plots) fused position estimate RMSEs are plotted. Compared to the results shown in Fig. 5, here the errors start to increase more rapidly at medium loss

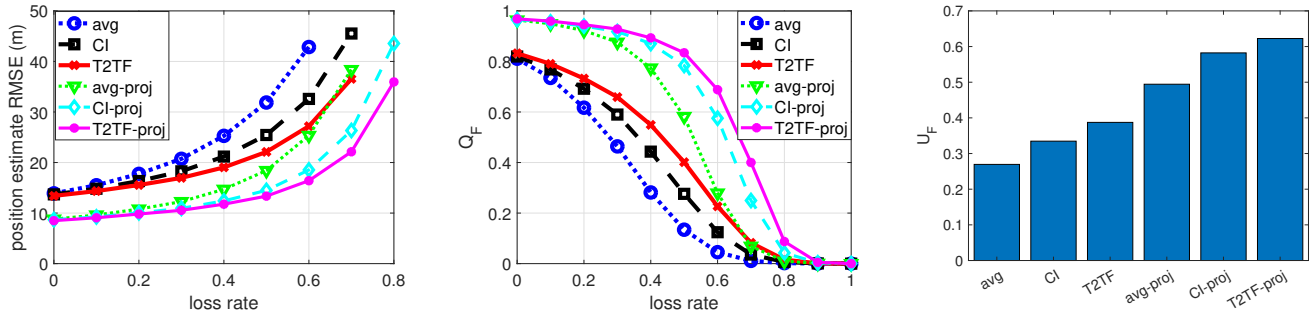

(a) RMSE (b) Q-p map (c) U_F

Fig. 7. Performance of fused position estimates with elliptical motion constraints

rates, reflecting the overall higher convexity of the $\mathcal{E}(p)$ curves compared to those in the former case. Besides, for either unconstrained or constrained errors, the same order of performance is seen: the T2TF performs best, followed by the CI fuser and AF.

For the mapping function, suppose we have again selected the reference error $\mathcal{E}_H$ to be $20\,\mathrm{m}$ and $\alpha = 4$, $\beta = 1$ based on system quality requirements. The one-step projection can reduce the errors variably by 30-40% compared to their unconstrained counterparts. As can be seen from another perspective in Fig. 7b, for either the unconstrained or constrained group, the T2TF Q-p map exhibits the longest concave region and is therefore the most sustained in its quality with increasing loss rates. Finally, Fig. 7c shows the sorted utilities of the various fuser setups, in which one can see the lowest U_F of the unconstrained AF output is just above 0.25, whereas the highest U_F can be achieved by the constrained T2TF at over 0.6. Generally speaking, a higher U_F value indicates a better sustained Q-p map and later transition point p_T. From Fig. 7b, the worst-performing unconstrained AF already has a convex Q-p map at 40% loss, whereas the same does not happen for the constrained T2TF until 80% loss.

V. Conclusion

In this work, we proposed ways to map the actual tracking errors to a quality measure that is defined on $[0, 1]$ based on required system accuracy performance. We showed the monotonicity and concavity properties of the selected mapping function. In particular, the transition from concave to convex profiles in the chosen mapping function enable us to highlight the most critical performance region, thereby selecting a fuser that yields estimates of better quality and is robust against increasing communication loss. The proposed Q-p map and the overall utility measure can quantitatively describe and compare the overall resilience performance of various fusers in the presence of increasingly adverse communication constraints.

Future work may include incorporation of other communication constraints such as delay into the quality measure. Also of interest are ways to utilize predicted quality measures based on error covariances for making decisions such as the selection of sensors and/or estimates and also adaptation of estimation and fusion mechanisms and their parameters to yield fused estimates that match required system quality performance.

Acknowledgment

This work was funded by the Mathematics of Complex, Distributed, Interconnected Systems Program, Office of Advanced Computing Research, U.S. Department of Energy, and SensorNet Project of Office of Naval Research, and was performed at Oak Ridge National Laboratory managed by UT-Battelle, LLC for U.S. Department of Energy under Contract No. DE-AC05-00OR22725.

References

[1] Y. Bar-Shalom, P. K. Willett, and X. Tian. *Tracking and Data Fusion: A Handbook of Algorithms*. YBS Publishing, Storrs, CT, 2011.

[2] E. Blasch, P. Valin, and E. Bosse. Measures of effectiveness for high-level fusion. In *Proc. 13th International Conference on Information Fusion (FUSION)*, pages 1–8, Edinburgh, U.K., Jul. 2010.

[3] A. Chiuso and L. Schenato. Information fusion strategies and performance bounds in packet-drop networks. *Automatica*, 47:1304–1316, Jul. 2011.

[4] Z. Duan and X. R. Li. Constrained target motion modeling – part ii: circular track. In *Proc. 16th International Conference on Information Fusion (FUSION)*, pages 2153–2160, Istanbul, Turkey, 2013.

[5] S. J. Julier and J. K. Uhlmann. A non-divergent estimation algorithm in the presence of unknown correlations. In *Proc. American Control Conference (ACC)*, volume 4, pages 2369–2373, Albuquerque, NM, Jun. 1997.

[6] Q. Liu, K. Brigham, and N. S. V. Rao. Estimation and fusion for tracking over long-haul links using artificial neural networks. *IEEE Transactions on Signal and Information Processing over Networks*, 3(4):760–770, Dec. 2017.

[7] Q. Liu and N. S. V. Rao. On state estimation and fusion with elliptical constraints. In *Proc. 13th International Conference on Multisensor Fusion and Integration for Intelligent Systems (MFI)*, pages 85–90, Daegu, Korea, Nov. 2017.

[8] Q. Liu, N. S. V. Rao, and X. Wang. Staggered scheduling of sensor estimation and fusion for tracking over long-haul links. *IEEE Sensors Journal*, 16(15):6130–6141, Aug. 2016.

[9] Q. Liu, X. Wang, and N. S. V. Rao. Fusion of state estimates over long-haul sensor networks with random loss and delay. *IEEE/ACM Transactions on Networking*, 23(2):644–656, Apr. 2015.

[10] Q. Liu, X. Wang, N. S. V. Rao, K. Brigham, and B. V. K. Vijaya Kumar. Effect of retransmission and retrodiction on estimation and fusion in long-haul sensor networks. *IEEE/ACM Transactions on Networking*, 24(1):449–461, Feb. 2016.

[11] E. I. Silva and M. A. Solis. An alternative look at the constant-gain Kalman filter for state estimation over erasure channels. *IEEE Transactions on Automatic Control*, 58(12):3259–3265, Dec. 2013.

[12] Y. Wang and X. R. Li. Distributed estimation fusion with unavailable cross-correlation. *IEEE Transactions on Aerospace and Electronic Systems*, 48(1):259–278, Jan. 2012.